

See discussions, stats, and author profiles for this publication at: <https://www.researchgate.net/publication/51564623>

# Density Functional Theory Studies on Ice Nanotubes

ARTICLE *in* THE JOURNAL OF PHYSICAL CHEMISTRY A · AUGUST 2011

Impact Factor: 2.69 · DOI: 10.1021/jp203984z · Source: PubMed

---

CITATIONS

7

READS

33

4 AUTHORS, INCLUDING:



Mahesh Kumar Ravva

King Abdullah University of Science and Tec...

21 PUBLICATIONS 205 CITATIONS

[SEE PROFILE](#)



R. Parthasarathi

Joint BioEnergy Institute

93 PUBLICATIONS 2,337 CITATIONS

[SEE PROFILE](#)

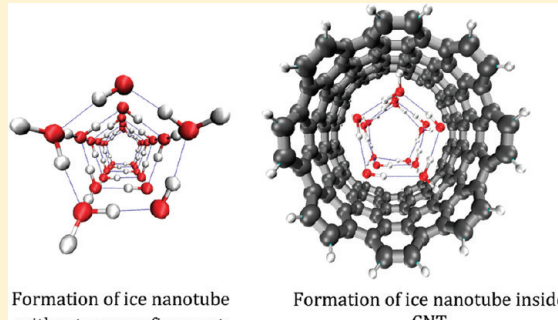
# Density Functional Theory Studies on Ice Nanotubes

R. Mahesh Kumar, M. Elango, R. Parthasarathi, and V. Subramanian\*

Chemical Laboratory, CSIR-Central Leather Research Institute, Adyar, Chennai 600 020, India

Supporting Information

**ABSTRACT:** The structure and stability of quasi one-dimensional (1D) ice nanotubes (INTs) have been investigated using Density Functional Theory (DFT) based Becke's three parameter Lee–Yang–Parr exchange and correlation functional (B3LYP) method employing various basis sets. Four different INTs, namely, (4,0)-INT, (5,0)-INT, (6,0)-INT, and (8,0)-INT with different lengths have been considered in this study. The calculated stabilization energies (SEs) illustrate that the stability of INT is proportional to its length and diameter. Further, the encapsulation of various gas molecules ( $\text{CO}_2$ ,  $\text{N}_2\text{O}$ , CO,  $\text{N}_2$ , and  $\text{H}_2$ ) inside the INTs has also been investigated. The calculated SEs of different endohedral complexes reveal that all these gas molecules are stable inside the tubes. The Bader's theory of atoms in molecule (AIM) has been used to characterize intra- and inter-ring H-bonding interactions. The electron density topological parameters derived from AIM theory brings out the difference between the intra- and inter-ring H-bonds of INTs.



The electron density topological parameters derived from AIM theory brings out the difference between the intra- and inter-ring H-bonds of INTs.

## ■ INTRODUCTION

The structure and stability of different water clusters have been extensively studied using both experimental and theoretical methods due to their importance in various branches of natural science.<sup>1–6</sup> Water is one of the few substances that occurs naturally in all three phases. Its solid phase is called ice, which can exist as amorphous or crystalline solid. Water molecules have two hydrogen atoms and two lone pairs enabling them to participate in four hydrogen bonds (H-bonds). The strong H-bonds are responsible for a variety of water clusters with different morphologies and crystalline ice structures. The role of H-bonding in the stabilization of hydrated crystal structures is well-known.<sup>7,8</sup> Furthermore, water has a space filling role in cases where there are cavities of a suitable size that arises due to the close packing of organic and inorganic molecules.<sup>9,10</sup>

Special attention has been paid to the water molecules in a confined environment in general and nanopores in particular.<sup>11–16</sup> Evidences from molecular dynamics simulations indicate that the water confined in nanotube of diameter less than 2 nm produces  $n$ -gonal structures formed of stacked rings at low temperature and high pressure.<sup>17,18</sup> When liquid water is encapsulated in carbon nanotubes, water molecules can align into certain quasi 1D structures due to the interplay of nanoscale confinement and strong H-bonding. These nanotubes are referred as ice nanotubes (INTs).<sup>12,18</sup>

The formation of various INTs has been investigated using diverse experimental techniques such as X-ray diffraction, neutron scattering, nuclear magnetic resonance, and vibrational spectroscopy.<sup>15,19–21</sup> Recently, Hodgson et al., have demonstrated the formation of a INT from pentagon rings on a planar metal surface. Results obtained from the combination of scanning

tunnelling microscopy (STM), reflection absorption infrared spectroscopy (RAIRS), and density functional theory (DFT) confirm that the ice chains are built from pentagon rings.<sup>22</sup> Bai et al. have shown that hexagonal tubes are more stable than the pentagonal ice nanotubes.<sup>23</sup> Theoretical studies have unveiled various nanoice-morphologies such as ladder-like INT, a helical INT, double- and triple-walled INT within carbon nanotube (CNT).<sup>24</sup> Koga and co-workers have investigated the possibility of the formation of INTs along with neon, argon, and methane as guest molecule inside the CNT. It has been shown that the attractive interaction of guest molecules stabilize the INT.<sup>25</sup>

Although computational studies have been carried out on encapsulation of INT inside the CNT, the investigations on the formation of such tubular structures in the absence of CNT are scarce. Hence, electronic structure calculations have been performed to understand the possibility of formation of the isolated INTs using different DFT methods employing various basis sets. Furthermore, the H-bonding interaction in various INTs has been characterized by using the Bader's theory of Atoms in Molecules (AIM) approach and vibrational analysis.<sup>26</sup> The following points have been addressed in this study.

- To determine the differences in the structure of INTs in the presence and absence of CNT confinement.
- To explore the inter-relationship between the stability and the length and diameter of the INTs.

**Special Issue:** Richard F. W. Bader Festschrift

**Received:** April 29, 2011

**Revised:** July 27, 2011

- (iii) To characterize the nature of inter- and intraring H-bonding interactions present in the formation of INTs.

## THEORETICAL BACKGROUND

**AIM Theory and Characterization of H-Bonds.** The molecular electron density distribution  $\rho(r)$  can be extracted from the corresponding many-particle wave function  $\psi(x_1, x_2, \dots, x_N)$  as

$$\rho(r) = N \sum_{\sigma} \int |\psi(x_1, x_2, \dots, x_N)|^2 d^3r_2, \dots, d^3r_N \quad (1)$$

Here, the summation runs over all spin coordinates, integration is over all but one spatial coordinate ( $x$  stands for position and spin), and  $N$  is the total number of electrons. Within the simplest Hartree–Fock framework wherein the wave function  $\psi$  is expressed in the form of a Slater determinant constructed from molecular orbitals that are, in turn, expressed as linear combinations of the basis functions  $\{\phi_i\}$ ,  $\rho(r)$  assumes the form

$$\rho(r) = \sum_{\mu\nu} P_{\mu\nu} \phi_{\mu}(r) \phi_{\nu}^{*}(r) \quad (2)$$

where  $P$  stands for the charge density–bond order matrix satisfying the idempotency condition. The electron density and Laplacian of electron density at bond critical point (BCP) are denoted  $\rho(r_c)$  and  $\nabla^2\rho(r_c)$ , respectively.

Bader and Essen have made the first study of the observed categories of critical points.<sup>27</sup> They concluded that the hallmark of “shared” (i.e., covalent) interactions is a high value of the charge density at BCP on the order of  $>10^{-1}$  au. The curvatures of the charge density are usually large. The Laplacian of the electron density ( $\nabla^2\rho(r_c)$ ) is a measure of local concentrations of density and may be positive or negative, on the order of  $\rho(r_c)$ . A negative Laplacian denotes electron concentration at a particular point, whereas a positive Laplacian implies depletion of charge. It is evident from the previous AIM analysis that in H-bonded systems, noble-gas dimers, and ionic systems,  $\rho(r_c)$  is quite small ( $\sim 10^{-2}$  au or less and  $10^{-3}$  au in van der Waals complexes) and the Laplacian is positive. These two observations are indicative of a closed-shell interaction.

Numerous studies have been made on various systems to characterize the different bonding interactions using the AIM theory.<sup>28,29</sup> Matta et al. have highlighted the applications of atomic properties derived from AIM theory and its importance in the prediction of experimentally measured quantities.<sup>30</sup> Popelier and colleagues have proposed several criteria to characterize the H-bonding interactions in various systems.<sup>31,32</sup> These include (1) correct topological pattern (BCP and gradient path), (2) appropriate values of electron density at BCP, (3) proper value of Laplacian of electron density at the BCP, and (4) mutual penetration of hydrogen and acceptor atoms. Criteria pertaining to integrated properties of hydrogen atoms involved in the H-bonding include (5) an increase of net charge, (6) an energetic destabilization, (7) a decrease in dipolar polarization, and finally, (8) a decrease in atomic volume.<sup>31,32</sup> Matta and Boyd have presented brief descriptions of the basic assumptions of the AIM approach.<sup>33</sup>

The topological descriptors obtained from the AIM theory can be successfully employed to distinguish weak, medium, and strong H-bonds in various molecular systems.<sup>34–38</sup> Grabowski et al. illustrated the covalent and noncovalent nature of various H-bonded complexes using Bader’s theory of electron density and interaction energy terms. It has been shown that the proton-acceptor

distance  $\sim 1.8$  Å and the ratio of delocalization and electrostatic terms  $\sim 0.45$  constitutes approximately a borderline between covalent and noncovalent hydrogen bonds.<sup>39</sup> During the same time, Parthasarathi et al. explained the borderless nature of hydrogen going from weak H-bonds to moderate and strong H-bonds using electron density at BCP.<sup>40</sup> Parthasarathi et al. have illustrated the usefulness of AIM theory to explain the nature of interaction in the first and second solvation shells and the presence of secondary interactions.<sup>41</sup> Grabowski and co-workers have made a detailed AIM analysis on H-bonded molecular systems.<sup>42,43</sup> Despite the greater variability of systems that are classified as H-bonds, it is possible to spell out criteria for the H-bonding interaction using the AIM theory. Based on the systematic analysis of several dimers, a new measure of H-bond strength ( $\Delta_{\text{com}}$ ) has been proposed using the properties of the proton donating bond. It is based on the geometrical and topological parameters of the X–H bond.<sup>44</sup>

$$\Delta_{\text{com}} = \left\{ \left[ \frac{(r_{\text{A}-\text{H}} - r_{\text{A}-\text{H}}^0)}{r_{\text{A}-\text{H}}^0} \right]^2 + \left[ \frac{(\rho_{\text{A}-\text{H}}^0 - \rho_{\text{A}-\text{H}})}{\rho_{\text{A}-\text{H}}^0} \right]^2 + \left[ \frac{(\nabla^2 \rho_{\text{A}-\text{H}} - \nabla^2 \rho_{\text{A}-\text{H}}^0)}{\nabla^2 \rho_{\text{A}-\text{H}}^0} \right]^2 \right\}^{1/2} \quad (3)$$

where  $r_{\text{A}-\text{H}}$ ,  $\rho_{\text{A}-\text{H}}$ , and  $\nabla^2 \rho_{\text{A}-\text{H}}$  correspond to the proton-donating bond involved in H-bonding, the bond length, electronic density at A–H bond critical point, and the Laplacian of this density, respectively;  $r_{\text{A}-\text{H}}^0$ ,  $\rho_{\text{A}-\text{H}}^0$ , and  $\nabla^2 \rho_{\text{A}-\text{H}}^0$  correspond to the same parameters of the A–H bond not involved in H-bond formation or any other nonbonded interaction. The usefulness of this parameter has been demonstrated in several studies.<sup>45–47</sup> In analogous fashion, Parthasarathi et al. defined a parameter for a complex containing several H-bonds as

$$\Delta_{\text{com}} = \left\{ \sum_{i=1}^n \left[ \frac{(r_{\text{A}-\text{H}} - r_{\text{A}-\text{H}}^0)}{r_{\text{A}-\text{H}}^0} \right]^2 + \sum_{i=1}^n \left[ \frac{(\rho_{\text{A}-\text{H}}^0 - \rho_{\text{A}-\text{H}})}{\rho_{\text{A}-\text{H}}^0} \right]^2 + \sum_{i=1}^n \left[ \frac{(\nabla^2 \rho_{\text{A}-\text{H}} - \nabla^2 \rho_{\text{A}-\text{H}}^0)}{\nabla^2 \rho_{\text{A}-\text{H}}^0} \right]^2 \right\}^{1/2} \quad (4)$$

It is worth clarifying that the summation of the above equation is over all the proton donating bonds in the H-bonded complex. Authors have validated the parameter for various water clusters.<sup>48</sup>

## COMPUTATIONAL DETAILS

**Description of Different Model Systems.** The nomenclature for the INTs is given based on the number of water molecules in the primary building unit (ring). For example, in the case of (4,0)-INT, each ring consists of four water molecules, with one OH group lying in the plane and the other oriented perpendicular to it. A more simple notation, INT<sub>n</sub><sup>m</sup> (where  $m$  = number of layers and  $n$  = number of water molecules in the ring), is used throughout the text. This notation implies that the INT is formed by  $m$ -layers of  $n$ -membered rings. With a view to understand the role of radius-dependent stability of INTs, DFT calculations were carried out on four different INTs, namely, (4,0)-INT, (5,0)-INT, (6,0)-INT, and (8,0)-INT. Further, to assess the effect of length on stability, four different layers (INT<sub>n</sub><sup>1</sup>, INT<sub>n</sub><sup>2</sup>, INT<sub>n</sub><sup>3</sup>, and INT<sub>n</sub><sup>6</sup>) were considered.

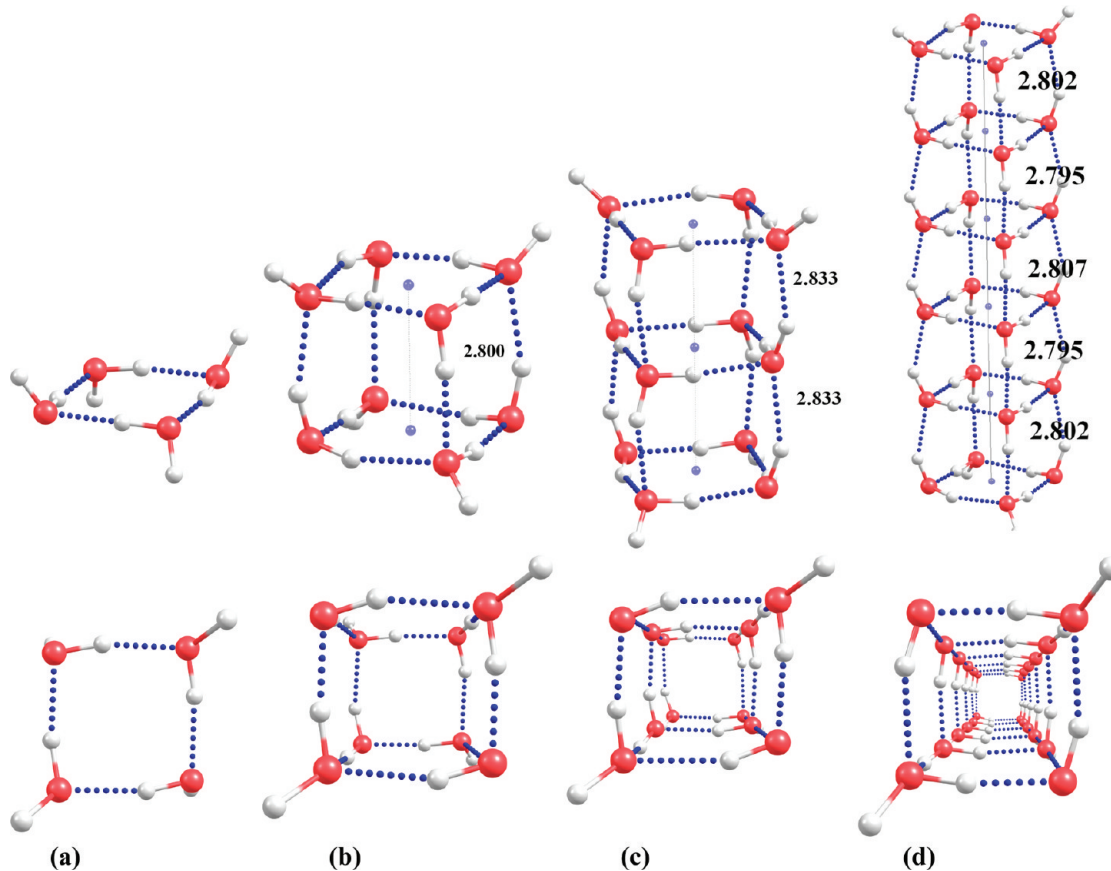


**Figure 1.** Optimized geometries of various (4,0)-INT complexes using the B3LYP/6-311G\*\* method. The dotted line represents the O–H···O hydrogen bond.

**Geometry Optimization of INT Complexes.** In the present study, the geometries of all INTs were optimized without any constraints using DFT(B3LYP) method<sup>49</sup> employing 6-311G\*\* basis set. To understand the role of nano confinement in the formation of INTs, two different INTs ((4,0) and (5,0)-INTs up to three layers) were optimized inside the CNTs using M05-2X functional<sup>50</sup> employing dual basis set. The CNT and INT atoms were treated using LANL2MB and 6-31+G\*\* basis sets, respectively.

**Calculation of Stabilization Energies.** The stabilization energy of INT ( $SE_{INT}$ ) in the absence of CNT confinement and the stabilization energy of endohedral complex formed by INT inside CNT were calculated using supermolecule approach and corrected for basis set superposition error (BSSE) following the procedure adopted by Boys and Bernardi.<sup>51</sup>

$$SE_{INT} = -(E_{\text{cluster}} - \sum_{i=1}^n E_i) \quad (5)$$

where  $E_{INT}$  and  $E_i$  are the total energies of INT and water molecule, respectively, and  $n$  is the total number of monomers in the INT. Specifically, BSSE was estimated for each water molecule in its location by computing with its own basis set and with the basis set for  $(n - 1)$ -mer. To understand the stability of INT further, the inter-ring stabilization energy (IRSE) was calculated using the following equation.

$$IRSE = -(E_{INT_n^m} - \sum_{i=1}^n E_{INT_n^{m-1}}) \quad (6)$$

where  $INT_n^m$  is the total energy of the  $m$  layers and  $INT_n^{m-1}$  is the total energy of the  $m - 1$  layers. Furthermore, various gas molecules encapsulated inside  $INT_8^3$  were also investigated. All endohedral complexes were fully optimized at the density functional theory (M05-2X) employing the 6-31+G\*\* basis set. Using these optimized geometries, SEs were calculated at MP2,<sup>52</sup> M06-2X,<sup>53</sup> and wb97x<sup>54</sup> employing the 6-311++G\*\* basis set using the following equation.

$$SE = -(E_{\text{complex}} - (E_{\text{mono1}} + E_{\text{mono2}})) \quad (7)$$

where  $E_{\text{complex}}$  is the total energy of the complex,  $E_{\text{mono1}}$  is the total energy of INT, and  $E_{\text{mono2}}$  corresponds to the total energy of the gas molecule. All calculations were carried out using the Gaussian 09 suite of programs.<sup>55</sup>

## RESULTS AND DISCUSSION

**Structure and Stability of INTs.** The optimized geometries of isolated INTs (in the absence of CNT) are presented in Figures 1–4. With a view to gain an insight into the structural difference between the geometries of the INTs in the presence and the absence of confinement, (4,0) and (5,0)-INTs with three layers were also optimized within (7,7) and (8,8)-CNTs, respectively. The optimized geometries of different INTs inside CNT are shown in Figure 5. The calculated H-bond distances and angles are presented in Supporting Information (Tables S1–S16). Examination of the results reveals that INTs can form stable tubular structures either inside CNT or in the absence of

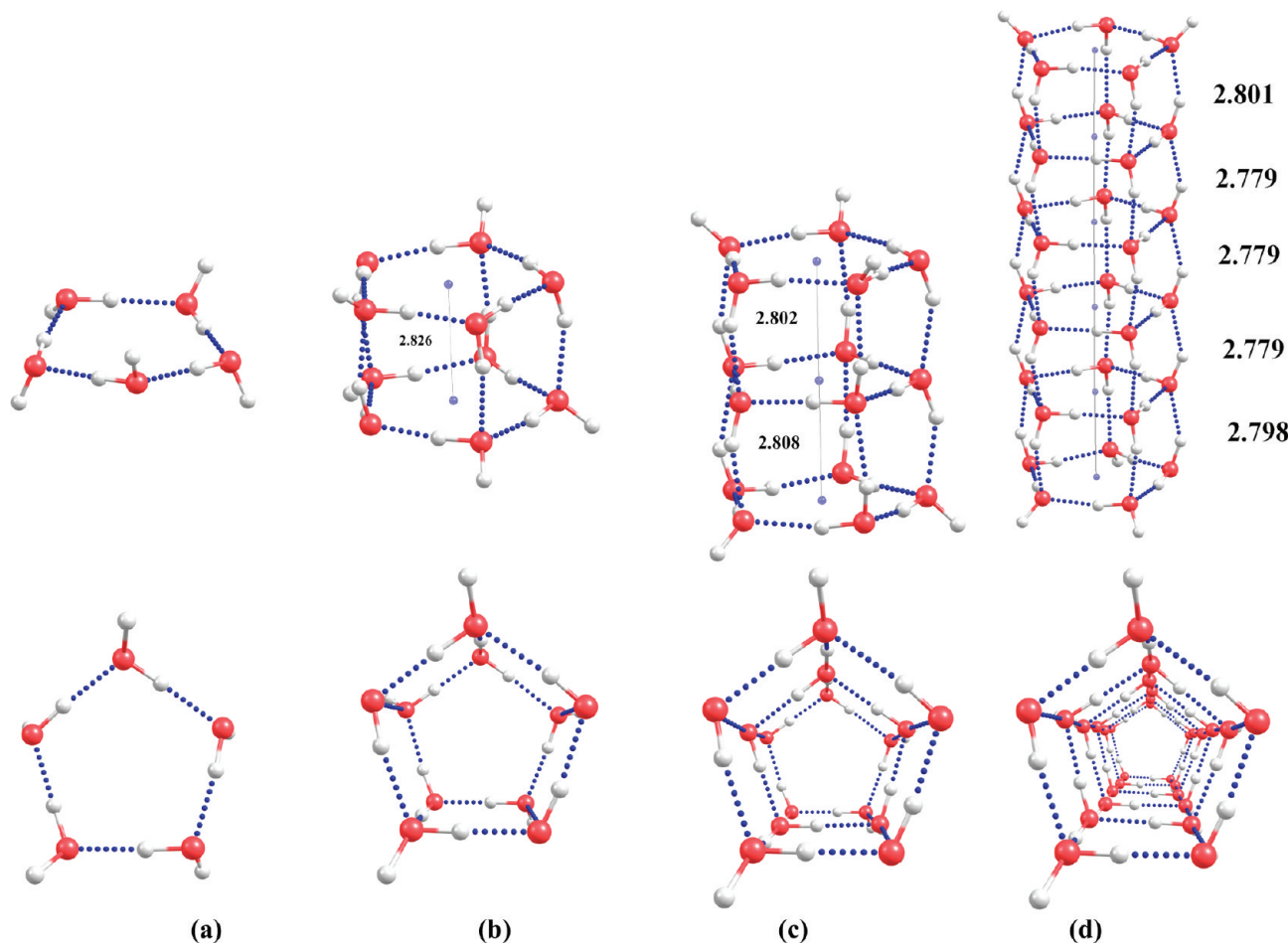


**Figure 2.** Optimized geometries of various (5,0)-INTs complexes using the B3LYP/6-311G\*\* method. The dotted line represents the HO $\cdots$ H hydrogen bond.

CNT confinement. There are no significant changes in the geometrical parameters of INT in the absence and in the presence of CNT confinement. This evidence shows that (7,7)-CNT and (8,8)-CNT can accommodate (4,0)-INT and (5,0)-CNT, respectively. The optimization of (5,0)-INT inside the (7,7)-CNT shows disruption in the structure of the water tube. These findings demonstrate that the optimal size of the water tube that can be incarcerated inside the (7,7)-CNT is (4,0)-INT.

It can be observed from the Figure 1 that the stacking of H-bonded water rings leads to the formation of a tube. In fact, the stacking of H-bonded water rings involves inter-ring H-bonding interaction (between two neighbor layers). The primary building block of the tube (4,0)-INT is water tetramer ( $\text{INT}_4^1$ ). In this arrangement, water tetramer exhibits  $S_4$  symmetry. The H-bonded ring contains nearly a planar O $\cdots$ O $\cdots$ O $\cdots$ O arrangement with free O–H bonds alternating up and down orientations with respect to this plane. The optimized geometry of  $\text{INT}_4^6$  is shown in Figure 1d along with the inter-ring distances. Close analysis of the  $\text{INT}_4^6$  geometry suggests that six layers of water tetramer can form a tubular structure. In this tubular arrangement, each water molecule acts as a double donor and double acceptor of the H-bond to satisfy the ice rule and can also form an infinitely long tubular structure. It can be found that one of the O–H group points along the axis of the water tube and the

other is perpendicular to the same. The number of H-bonds present in between the two neighbor rings is equal to the number of water molecules in the basic building block. As the length of the tube increases, the inter-ring distance decreases. A similar observation has also been found in the linear water chain.<sup>56</sup> In  $\text{INT}_4^6$ , stacked layers that are present inside the tube have shorter inter-ring distances than that of terminal layers.

The formation of larger tubular structures is based on the n-gonal water rings. Figure 2 illustrates the tubular structure of  $\text{INT}_5^6$ , which is built from a pentagonal water ring. In  $\text{INT}_5^1$ , five water molecules are hydrogen bonded in cyclic fashion. Figure 2 reveals that  $\text{INT}_5^6$  is formed from the stacking of six water pentamer units. Similarly, six and eight water rings are H-bonded and stacked to form  $\text{INT}_6^6$  and  $\text{INT}_8^6$ . Overall, the geometrical parameters elicit that as the size of the tube increases, there are no noticeable changes in the inter-ring H-bonded distances and all the water tubes satisfy the ice rule.<sup>11</sup>

The calculated BSSE corrected SEs of INTs at the B3LYP/6-311++G\*\* level of theory are reported in Table 1 along with the number of H-bonds ( $N_H$ ). SE/H-bonds (SE/ $N_H$ ) are also listed in the same table. SEs for  $\text{INT}_4^1$ ,  $\text{INT}_4^2$ ,  $\text{INT}_4^3$ , and  $\text{INT}_4^6$  shows that the stability of the tube increases with an increase in the length. These results were extrapolated to infinity using oligomeric approach to derive the SE and IRSE for the tube of infinite size ( $\text{INT}_4^\infty$ ; see Supporting Information, Figure S1). The SE for

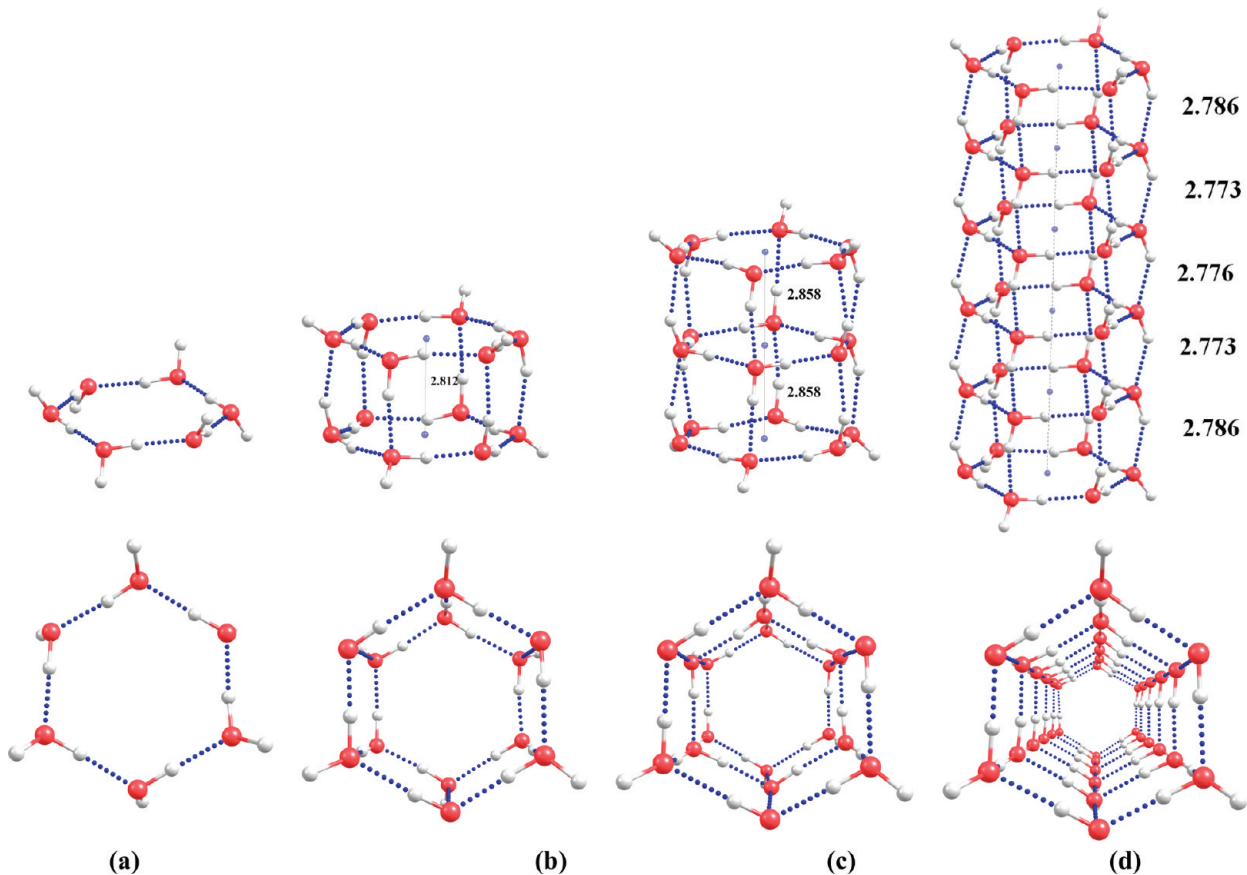


**Figure 3.** Optimized geometries of various (6,0)-INT complexes using the B3LYP/6-311G\*\* method. The dotted line represents the HO $\cdots$ H hydrogen bond.

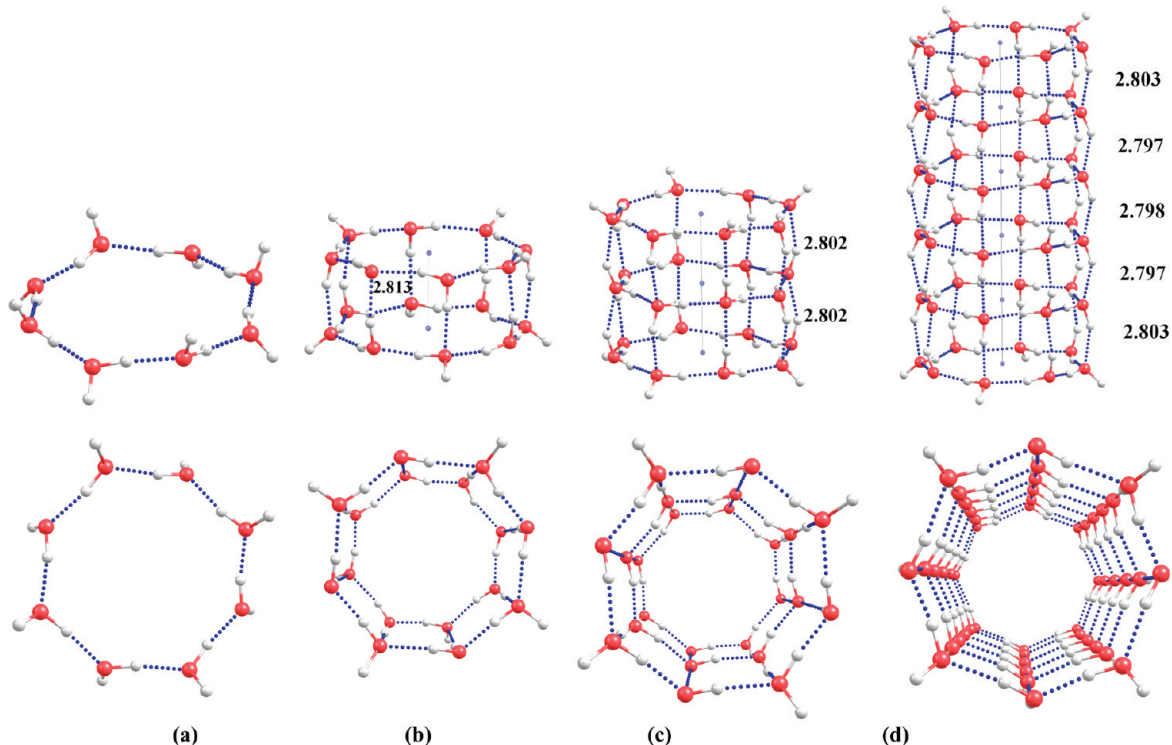


**Figure 4.** Optimized geometries of various (8,0)-INT complexes using the B3LYP/6-311G\*\* method. The dotted line represents the HO $\cdots$ H hydrogen bond.

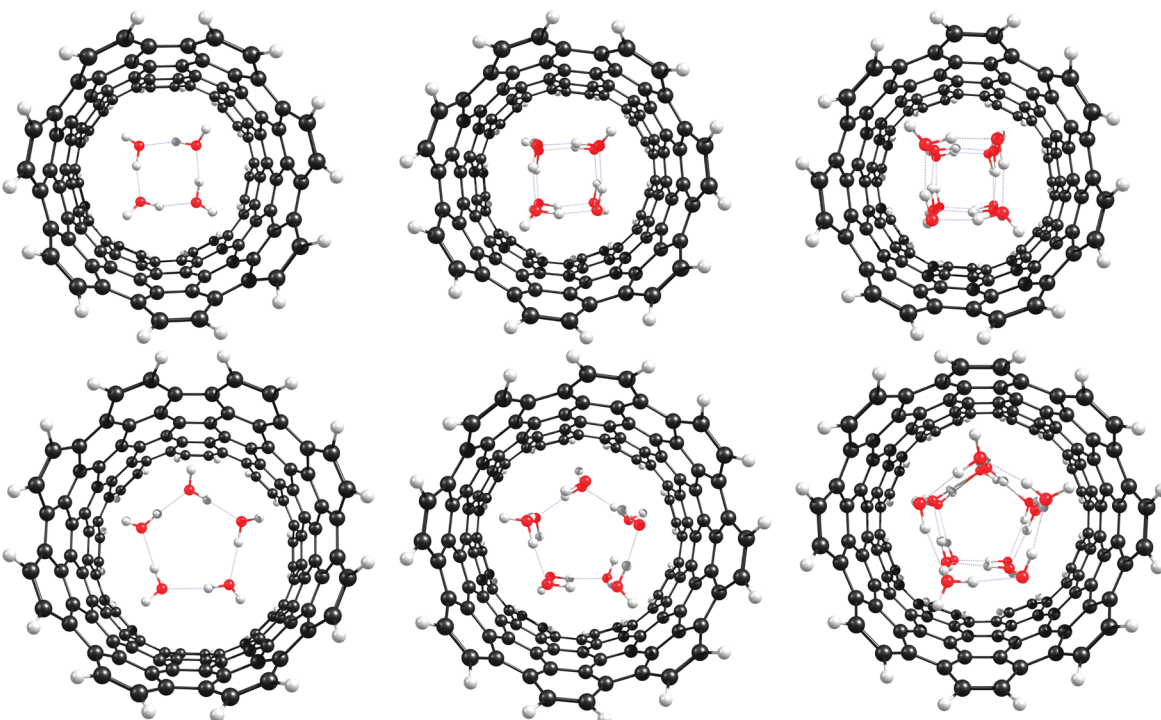


**Figure 5.** Optimized geometries of various (4,0) and (5,0) INT complexes encapsulated inside the CNT using M052X/(LANL2MB U 6-31+G\*\*) method. The dotted line represents the HO $\cdots$ H hydrogen bond.

**Table 1. Calculated Stabilization Energies (SEs) and Inter-Ring Stabilization Energies (IRSE) of Various INT Complexes at the B3LYP/6-311+G\*\* Level of Theories (kcal/mol)**

	isolated INTs		INTs inside CNT				isolated INTs		INTs inside CNT	
	SE	SE/H-bond	SE	SE/H-bond	No. of H-bonds	IRSE	IRSE/H-bond	IRSE	IRSE/H-bond	No. of H-bonds
INT <sub>4</sub> <sup>1</sup>	27.9	6.9	27.7	6.9	4					
INT <sub>4</sub> <sup>2</sup>	72.4	6.0	70.8	5.9	12	19.2	4.8	16.9	4.2	4
INT <sub>4</sub> <sup>3</sup>	113.6	5.6	109.2	5.4	20	35.2	4.4	29.5	3.6	8
INT <sub>4</sub> <sup>6</sup>	255.4	5.8			44	87.8	4.3			20
INT <sub>5</sub> <sup>1</sup>	37.0	7.3	33.7	6.7	5					
INT <sub>5</sub> <sup>2</sup>	93.5	6.2	86.8	5.7	15	23.3	4.6	21.4	4.2	5
INT <sub>5</sub> <sup>3</sup>	145.5	5.8	134.4	5.3	25	40.2	4.0	40.6	4.0	10
INT <sub>5</sub> <sup>6</sup>	307.5	5.5			55	98.0	3.9			25
INT <sub>6</sub> <sup>1</sup>	46.22	7.7			6					
INT <sub>6</sub> <sup>2</sup>	115.2	6.4			18	27.0	4.5			6
INT <sub>6</sub> <sup>3</sup>	179.2	5.9			30	47.5	3.9			12
INT <sub>6</sub> <sup>6</sup>	369.1	5.5			66	105.9	3.5			30
INT <sub>8</sub> <sup>1</sup>	61.0	7.6			8					
INT <sub>8</sub> <sup>2</sup>	151.0	6.2			24	36.6	4.5			8
INT <sub>8</sub> <sup>3</sup>	230.9	5.7			40	59.5	3.7			16
INT <sub>8</sub> <sup>6</sup>	532.6 <sup>a</sup>	6.0 <sup>a</sup>			88	136.5	3.4			40

<sup>a</sup> BSSE uncorrected values.

the infinitely long tube from water tetramer is 402.0 kcal/mol. The SE/ $N_H$  ranges from 5.8 to 6.9 kcal/mol. The calculated IRSE varies from 19.2 to 87.8 kcal/mol. The IRSE for the infinitely long tube is 140.0 kcal/mol (see Supporting Information, Figure S2). The range of IRSE per H-bond (IRSE/ $N_H$ ) is 4.3–4.8 kcal/mol. With an increase in the size of the tube, enhancement in the SE and IRSE can be observed, implying the increase in the overall

stability of the tubular structures. However, both SE/ $N_H$  and IRSE/ $N_H$  decrease with an increase in the length of the tubular structure. Further, it can be observed that the decrease in the SE/ $N_H$  is more rapid for INT<sub>8</sub><sup>1</sup> when compared to other systems due to its size.

To understand the role of confinement in the formation of INTs, the SEs and IRSEs of various INTs (optimized inside CNT) were

calculated. The calculated energies are depicted in Figure 6. It can be noticed that there are no significant changes in these values due to structural confinement. This may be attributed to the fact that the sizes of CNTs are optimal for hosting the water tubular structures. Further, the analysis reveals that the diameters of (7,7)-CNT and (8,8)-CNT are 9.62 and 11.05 Å and are sufficient to incarcerate these INTs inside CNT.

**Vibrational Analysis.** With a view to characterize the H-bonding interaction in INTs, the O–H stretching frequencies of INTs lying inside CNT and isolated INTs were calculated at the B3LYP/6-311G\*\* level and the results are presented in Table 2. It is clear from optimized geometries that INTs contain two types of H-bonds, namely, intramolecular (with in the ring) and inter-ring (between the rings) H-bonding interactions. The O–H stretching frequencies of intramolecular H-bonds are similar to that of bulk water, while inter-ring H-bonds are different from conventional H-bonds. The same observations have also been found in the previous experimental and theoretical studies on the similar systems.<sup>57</sup> The careful analysis of vibrational frequencies reveals that intramolecular H-bonds are stronger than that of inter-ring H-bonds in concomitant with the SE parameters. It is

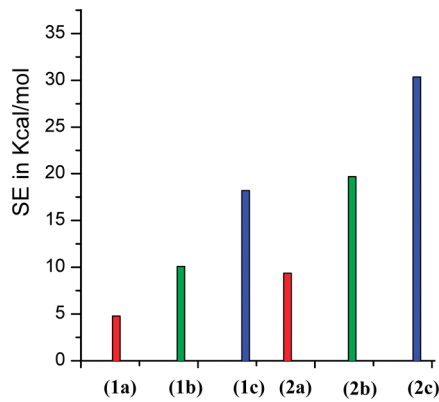


**Figure 6.** Calculated SE for (1a) INT<sub>4</sub><sup>1</sup>, (1b) INT<sub>4</sub><sup>2</sup>, and (1c) INT<sub>4</sub><sup>3</sup> inside (7,7)-CNT and (2a) INT<sub>5</sub><sup>1</sup>, (2b) INT<sub>5</sub><sup>2</sup>, and (2c) INT<sub>5</sub><sup>3</sup> inside (8,8)-CNT.

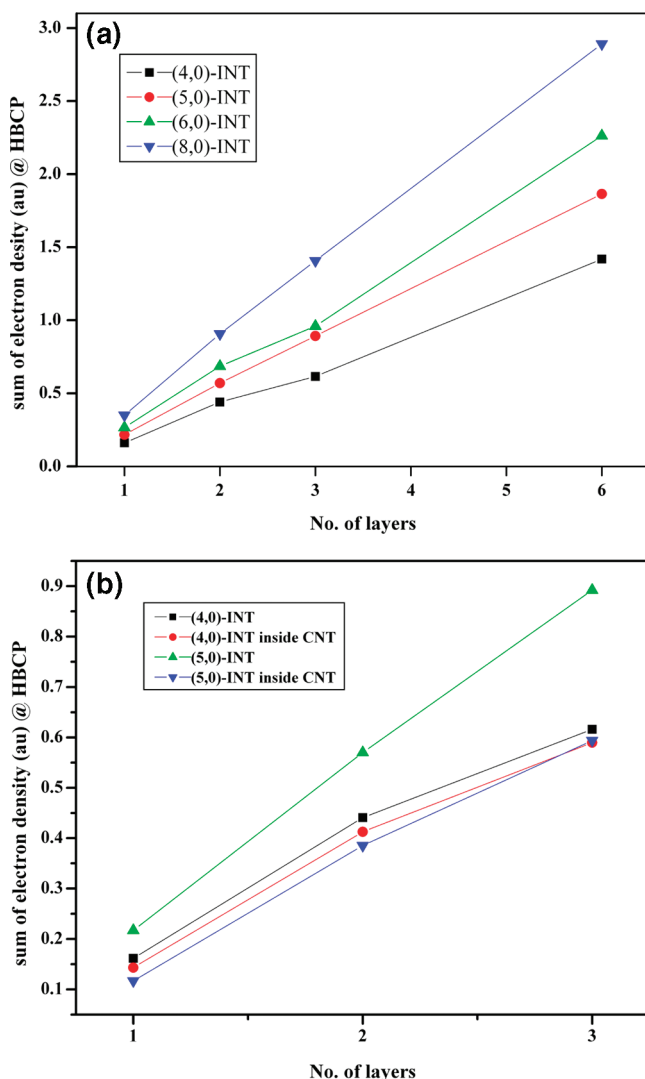


**Figure 7.** Calculated sum of electron density at HBCP for (a) isolated INTs and (b) isolated INTs and INTs inside CNT.

**Table 2. Calculated Ranges of Vibrational Frequency of Various INT Complexes at the B3LYP/6-311G\*\* Level of Theory (cm<sup>-1</sup>)**

system	isolated INTs			INTs inside CNT		
	intra	inter	free	intra	inter	free
INT <sub>4</sub> <sup>1</sup>	3317–3483		3866	3431–3563		3878–3914
INT <sub>4</sub> <sup>2</sup>	3171–3660	3171	3600–3660	3876	3229–3779	3877–3889
INT <sub>4</sub> <sup>3</sup>	3230–3716	3230–3481	3638–3716	3874–3882	3303–3757	3861–3888
INT <sub>4</sub> <sup>6</sup>	3161–3706	3161–3600	3600–3706	3871		
INT <sub>5</sub> <sup>1</sup>	3259–3442			3870–3877	3581–3680	3875–3890
INT <sub>5</sub> <sup>2</sup>	3036–3711	3036–3564	3582–3711	3874–3880	3439–3811	3887–3928
INT <sub>5</sub> <sup>3</sup>	3013–3733	3013–3567	3616–3730	3866–3874	3469–3825	3635–3781
INT <sub>5</sub> <sup>6</sup>	3000–3730	3000–3485	3555–3730	3871–3884		3836–3865
INT <sub>6</sub> <sup>1</sup>	3251–3445			3877		
INT <sub>6</sub> <sup>2</sup>	3050–3655	3050–3126	3568–3655	3874		
INT <sub>6</sub> <sup>3</sup>	3218–3716	3218–3468	3600–3716	3874		
INT <sub>6</sub> <sup>6</sup>	3170–3704	3170–3567	3600–3700	3879		
INT <sub>8</sub> <sup>1</sup>	3277–3466			3862–3874		
INT <sub>8</sub> <sup>2</sup>	3097–3661	3097–3588	3591–3661	3847–3872		
INT <sub>8</sub> <sup>3</sup>	3180–3698	3180–3439	3600–3698	3870		
INT <sub>8</sub> <sup>6</sup>	3177–3712	3177–3500	3500–3712	3870		

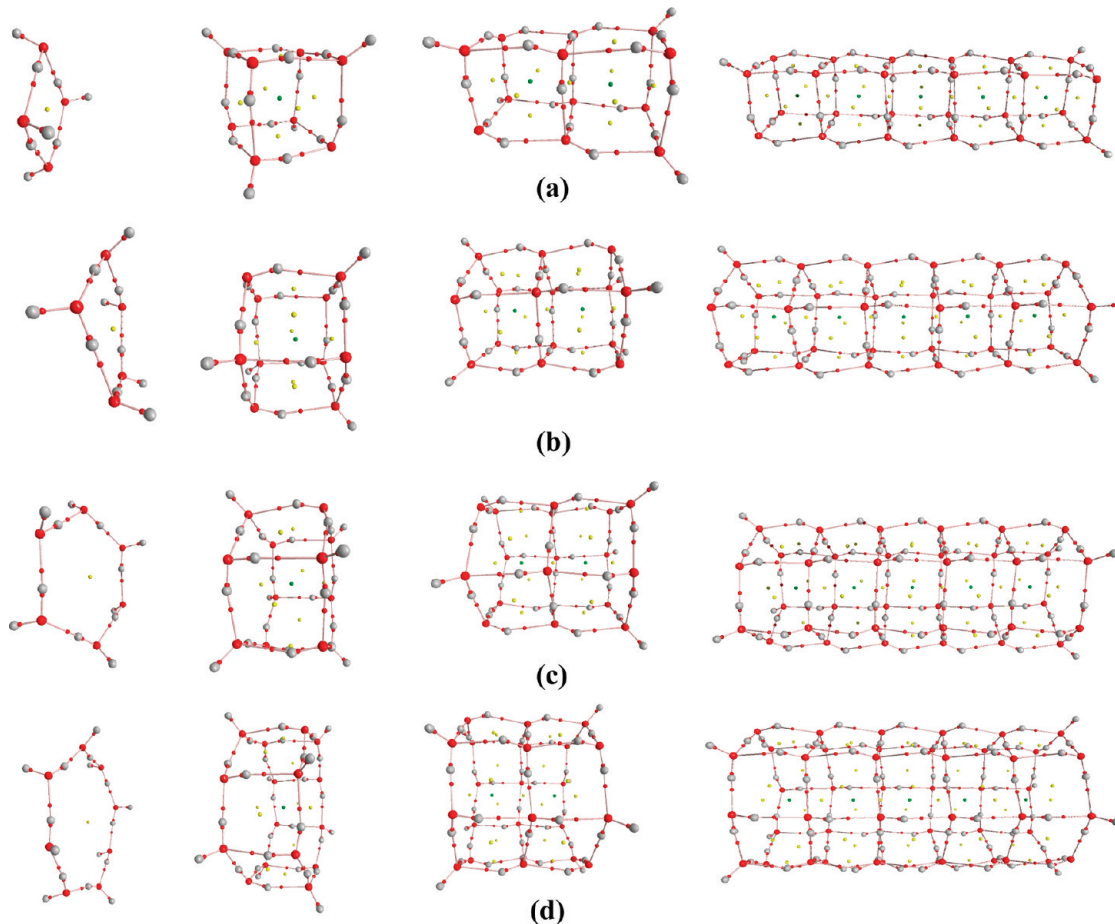


**Figure 8.** Molecular graphs of (a) (4,0)-INT, (b) (5,0)-INT, (c) (6,0)-INT, and (d) (8,0)-INT complexes.

interesting to note that as the length of the tubular structure increases the O–H stretching frequency decreases. All O–H stretching frequencies exhibit red shift. Reduced red shift in the O–H stretching frequencies has been observed in the INTs, which are optimized inside the CNT (Table 2).

**AIM Analysis.** The wave functions generated from the B3LYP/6-311++G\*\* level of calculations were used to generate the molecular graphs of all INT complexes. The calculated sum of electron density ( $\Sigma\rho(r_c)$ ) of various INTs are depicted in Figure 7. Calculated various topological parameters of all INTs at HBCP were given in Supporting Information, Tables S1–S16. AIM calculations were carried out using the AIM 2000 package.<sup>58</sup> The molecular graphs of various systems are shown in Figure 8. In this figure, the BCPs (bond critical points), RCPs (ring critical points), and CCPs (cage critical points) are represented as red, yellow, and green circles, respectively. All these values satisfy the topological criteria for the existence of H-bonding interaction.<sup>31,52</sup> It can be seen from the Supporting Information (Tables S1–S16) that the values of electron density and its Laplacian are useful to distinguish between intramolecular and inter-ring H-bonds. Considerable differences are observed between the intra- and intermolecular HBCPs. Larger values have been found at the HBCP of intraring H-bonds than the inter-ring H-bonds. Thus, intraring H-bonds are stronger than that of inter-ring H-bonds. Also, as the size of the ring increases, HBCP values increase. As mentioned in previous reports, there is a linear relationship between the electron density at HBCP and the strength

of the interaction ( $R^2 = 0.99$ ).<sup>52</sup> It can be seen from the molecular graphs that, for each HO $\cdots$ H interaction, there exists a bond path linking the H atom of the water molecule with the oxygen atom of another water molecule.

The interatomic and intermolecular interactions have been characterized with the aid of the local electron energy density ( $H_C$ ) and its components, the local kinetic electron energy density ( $G_C$ ) and local potential electron energy density ( $V_C$ ) at the BCPs. The relation between these energetic parameters is given in the eq 8.

$$H_C = G_C + V_C \quad (8)$$

Further, from the viral theorem that

$$\frac{1}{4}\nabla^2\rho_C = 2G_C + V_C \quad (9)$$

The balance between the local kinetic electron energy density ( $G_C$ ) and the local potential electron energy density ( $V_C$ ) reveal the nature of the interaction. If the ratio,  $-G_C/V_C$ , is greater than 1, then the nature of the interaction is purely noncovalent. It can be seen from the Supporting Information (Tables S1–S16) that as the intraring size increases the value of  $-G_C/V_C$  also decreases, that is, covalency of the H-bond decreases. A similar observation is also made in the case of inter-ring H-bonds. As the length of the tube increases, a decrease in the  $-G_C/V_C$  has been observed.

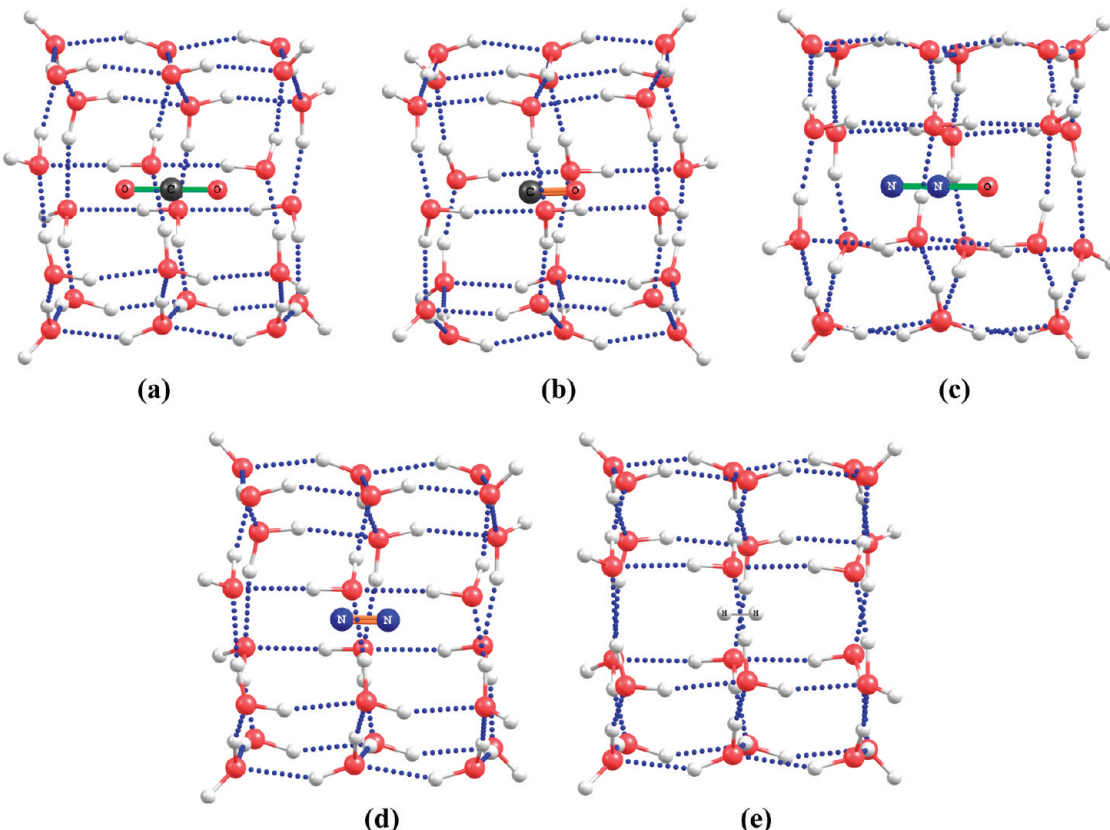


**Figure 9.** Optimized geometries of various gas molecules (a)  $\text{CO}_2$ , (b)  $\text{CO}$ , (c)  $\text{N}_2\text{O}$ , (d)  $\text{N}_2$ , and (e)  $\text{H}_2$  encapsulated in (8,0)-INT complexes using the M052X/6-31+G\*\* method. The dotted line represents the  $\text{HO}\cdots\text{H}$  hydrogen bond.

**Table 3. Calculated Stabilization Energies (SEs) of Various Gas Molecules Encapsulated in  $\text{INT}_8^3$  Using MP2/6-31++G\*\*, M06-2X/6-31++G\*\*, and wB97x/6-31++G\*\* Levels of Theory (kcal/mol)**

gas molecules	M06-2X	wB97x	MP2
$\text{N}_2\text{O}$	6.5	5.3	4.4
$\text{CO}_2$	6.2	5.2	3.6
$\text{CO}$	3.9	2.9	1.5
$\text{N}_2$	3.4	3.5	1.3
$\text{H}_2$	1.4	1.8	0.5

**Applications of INTs.** Clathrate hydrates are inclusion compounds that incorporate guest molecules inside the polyhedral cages of the host framework made up of H-bonded water molecules.<sup>59</sup> Hence, the uses of clathrate hydrates for hydrogen storage applications have received widespread attention by researchers. Recently, the possibility of clathrate hydrates as  $\text{CO}_2$  capturing agents has been investigated using electronic structure methods.<sup>60</sup> Prompted by these studies, the usefulness of INTs for storing and separation of various gas molecules such as  $\text{H}_2$ ,  $\text{N}_2$ ,  $\text{CO}$ ,  $\text{N}_2\text{O}$ , and  $\text{CO}_2$  has been explored. The gas molecule incarcerated INTs were optimized using the M05-2X/6-31+G\*\* method. The optimized geometries of the gas molecules encapsulated INT complexes are given in Figure 9. It can be seen that all gas molecules lie at the center of the water tube. There are no significant changes in the structure of INTs due to the encapsulation of these gas molecules. The calculated SEs at

MP2, M06-2X, and wB97x employing the 6-311++G\*\* basis set on M05-2X/6-31+G\*\* method optimized geometries are listed in Table 3. These values reveal that all gas molecules are stable inside the INTs. It can be seen from the results that, among all complexes, the SE of the  $\text{N}_2\text{O}$  encapsulated INT is the highest. The calculated SEs of various complexes show that all these gas molecules are stable inside the INT. Examination of the results elicits that the interaction between the two systems is dispersion dominant. Both M06-2X and wB97x functionals overestimate MP2 values. The molecular graphs derived from the AIM analysis are depicted in the Supporting Information (Figure S1). The calculated electron density at weak bond CP (WBCP) along with its Laplacian is given in the Supporting Information (Table S17). The molecular graphs involving the gas molecules and the tube structure indicate the role of the nonbonded interaction in the stabilization of gas molecules inside the INTs. The stabilization energy of the complexes bears a linear relationship with the sum of  $\rho(r_c)$  at WBCPs ( $R^2 = 0.92$ ). The correlation coefficient is close to unity. The same linear relation has also been observed between the SE and the sum of  $\nabla^2\rho(r_c)$  at WBCPs.

## CONCLUSIONS

The DFT-based B3LYP method along with different basis sets have been used to unravel the structure and stability of isolated INTs and the same inside the CNT. The calculated stabilization energies show that the INTs are stable without any structural confinement. However, the appropriate size of the CNT is important to stabilize the INTs inside the same. The results elucidate that SE is higher than the IRSE. Nevertheless, intra- and

inter-ring interactions are significantly important factors in the stabilization of the INTs. The results derived from the encapsulation of various gas molecules show that gas molecules are stable inside the INTs. The Bader's theory of AIM differentiates the strength of intra- and inter-ring H-bonding interactions that orchestrate the formation of INTs.

## ■ ASSOCIATED CONTENT

**Supporting Information.** Calculated geometrical parameters along with the topological parameters at HBCP of all INTs and molecular graphs of various gas molecules encapsulated inside INTs. This material is available free of charge via the Internet at <http://pubs.acs.org>.

## ■ AUTHOR INFORMATION

### Corresponding Author

\*Tel.: +91 44 24411630. Fax: +91 44 24911589. E-mail: subuchem@hotmail.com, subbu@clri.res.in.

## ■ ACKNOWLEDGMENT

Authors dedicate this article to R. F. W. Bader on the occasion of his 80th birthday. R.M.K wishes to thank Council of Scientific and Industrial Research (CSIR), New Delhi, India, for a senior research fellowship. Authors thank the CSIR network program of Centre for Excellence project (NWP-53) for financial support.

## ■ REFERENCES

- (1) Pauling, L. *The Nature of the Chemical Bond*; Cornell University Press: Ithaca, NY, 1960.
- (2) Jeffrey, G. A.; Saenger, W. *Hydrogen Bonding in Biology and Chemistry*; Springer-Verlag: Berlin, 1991.
- (3) Buckingham, A. D.; Legon, A. C.; Roberts, S. M. *Principles of Molecular Recognition*; Blackie Academic and Professional: London, 1993.
- (4) Jeffrey, G. A. *An Introduction to Hydrogen Bonding*; Oxford University Press: New York, 1997.
- (5) Scheiner, S. *Hydrogen Bonding. A Theoretical Perspective*; University Press: Oxford, U.K., 1997. Steiner, T. *Angew. Chem., Int. Ed.* **2002**, *41*, 48.
- (6) Parthasarathi, R.; Subramanian, V. *Characterization of Hydrogen Bonding: from van der Waals Interactions to Covalency, in Hydrogen Bonding-New Insight: Challenges and Advances in Computational Chemistry and Physics Series*, Kluwer, Amsterdam, 2006; pp 1–50.
- (7) Desiraju, G. R. *J. Chem. Soc., Chem. Commun.* **1991**, 426–428.
- (8) Clarke, H. D.; Arora, K. K.; Bass, H.; Kavuru, P.; Ong, T. T.; Pujari, T.; Wojtas, L.; Zaworotko, M. J. *J. Cryst. Growth Des.* **2010**, *10*, 2152–2167.
- (9) Custelcean, R.; Afloraei, C.; Vlassa, M.; Polverejan, M. *Angew. Chem., Int. Ed.* **2000**, *39*, 3094–3096.
- (10) Varughese, S.; Desiraju, G. R. *J. Cryst. Growth Des.* **2010**, *10*, 4184–4196.
- (11) Buch, V.; Devlin, J. P. *Water in Confining Geometries*; Springer: Berlin, NY, 2003.
- (12) Koga, K.; Gao, G. T.; Tanaka, H.; Zeng, X. C. *Nature* **2001**, *412*, 802–805.
- (13) Hummer, G.; Rasaiah, J. C.; Noworyta, J. P. *Nature* **2001**, *414*, 188–190.
- (14) Noon, W. H.; Ausman, K. D.; Smalley, R. E.; Ma, J. P. *Chem. Phys. Lett.* **2002**, *355*, 445–448.
- (15) Kolesnikov, A. I.; Zanotti, J. M.; Loong, C. K.; Thiagarajan, P.; Moravsky, A. P.; Loutfy, R. O.; Burnham, C. *J. Phys. Rev. Lett.* **2004**, *93*, 035503–4.
- (16) Mashl, R. J.; Joseph, S.; Aluru, N. R.; Jakobsson, E. *Nano Lett.* **2003**, *3*, 589–592.
- (17) Koga, K.; Parra, R. D.; Tanaka, H.; Zeng, X. C. *J. Chem. Phys.* **2000**, *113*, 5037–4.
- (18) Koga, K.; Gao, G. T.; Tanaka, H.; Zeng, X. C. *Phys. A* **2002**, *314*, 462–469.
- (19) Maniwa, Y.; Kataura, H.; Abe, M.; Suzuki, S.; Achiba, Y.; Kira, H.; Matsuda, K. *J. Phys. Soc. Jpn.* **2002**, *71*, 2863–2866.
- (20) Maniwa, Y.; Kataura, H.; Abe, M.; Udaka, A.; Suzuki, S.; Achiba, Y.; Kira, H.; Matsuda, K.; Kadokawa, H.; Okabe, Y. *Chem. Phys. Lett.* **2005**, *401*, 534–538.
- (21) Ghosh, S.; Ramanathan, K. V.; Sood, A. K. *Europhys. Lett.* **2004**, *65*, 678–684.
- (22) Carrasco, J.; Michaelides, A.; Forster, M.; Haq, S.; Raval, R.; Hodgson, A. *Nat. Mater.* **2009**, *8*, 427–431.
- (23) Bai, J.; Su, C. R.; Parra, R. D.; Zeng, X. C.; Tanaka, H.; Koga, K.; Li, J. M. *J. Chem. Phys.* **2003**, *118*, 3913–4.
- (24) Bai, J.; Wang, J.; Zeng, X. C. *Proc. Natl. Acad. Sci. U.S.A.* **2006**, *103*, 19664–19667.
- (25) Tanaka, H.; Koga, K. *J. Chem. Phys.* **2005**, *123*, 094706–6.
- (26) Bader, R. F. W. *Atoms in Molecules: A Quantum Theory*; Clarendon Press: Oxford, U.K., 1990.
- (27) Bader, R. F. W.; Essen, H. *J. Chem. Phys.* **1984**, *80*, 1943–18.
- (28) Popelier, P. L. A. *Atoms in Molecules: An Introduction*; Prentice Hall, Pearson Education Limited: New York, 2000.
- (29) Walker, V. E. J.; Castillo, N.; Matta, C. F.; Boyd, R. J. *J. Phys. Chem. A* **2010**, *114*, 10315–10319.
- (30) Matta, C. F.; Bader, R. F. W. *J. Phys. Chem. A* **2006**, *110*, 6365–6371.
- (31) Koch, U.; Popelier, P. L. A. *J. Phys. Chem.* **1995**, *99*, 9747–9754.
- (32) Popelier, P. L. A. *J. Phys. Chem. A* **1998**, *102*, 1873–1878.
- (33) Matta, C. J.; Boyd, R. J. An Introduction to the Quantum Theory of Atoms in Molecules. In *Quantum Theory of Atoms in Molecules: Recent Progress in Theory and Application*; Matta, C. J., Boyd, R. J., Eds.; Wiley-VCH: New York, 2007; Chapter I.
- (34) Cubero, E.; Orozco, M.; Hobza, P.; Luque, F. J. *J. Phys. Chem. A* **1999**, *103*, 6394–6401.
- (35) Luque, F. J.; Lopez, J. M.; de la Paz, M. L.; Vicent, C.; Orozco, M. *J. Phys. Chem. A* **1998**, *102*, 6690–6696.
- (36) Lipkowski, P.; Grabowski, S. J.; Leszczynski, J. *J. Phys. Chem. A* **2006**, *110*, 10296–10302.
- (37) Parthasarathi, R.; Amutha, R.; Subramanian, V.; Nair, B. U.; Ramasami, T. *J. Phys. Chem. A* **2004**, *108*, 3817–3828.
- (38) Sukhanov, O. S.; Shishkin, O. S.; Gorb, L.; Leszczynski, J. *Struct. Chem.* **2008**, *19*, 171–180.
- (39) Grabowski, S. J.; Sokalski, W. A.; Leszczynski, J. *J. Phys. Chem. A* **2006**, *110*, 4772–4779.
- (40) Parthasarathi, R.; Subramanian, V.; Sathyamurthy, N. *J. Phys. Chem. A* **2006**, *110*, 3349–3351.
- (41) Parthasarathi, R.; Subramanian, V.; Sathyamurthy, N. *J. Phys. Chem. A* **2007**, *111*, 13287–13290.
- (42) Sobczyk, L.; Grabowski, S. J.; Krygowski, T. M. *Chem. Rev.* **2011**, *105*, 3513–3560.
- (43) Grabowski, S. J. *Chem. Rev.* **2011**, *111*, 2597–2625.
- (44) Grabowski, S. J. *Chem. Phys. Lett.* **2001**, *338*, 361–366.
- (45) Grabowski, S. J. *J. Phys. Chem. A* **2001**, *105*, 10739–10746.
- (46) Grabowski, S. J.; Sokalski, W. A.; Leszczynski, J. *J. Phys. Chem. A* **2004**, *108*, 1806–1812.
- (47) Yurenko, Y. P.; Zhurakovskiy, R. O.; Ghomi, M.; Samijlenko, S. P.; Hovorun, D. M. *J. Phys. Chem. B* **2008**, *112*, 1240–1250.
- (48) Parthasarathi, R.; Subramanian, V.; Sathyamurthy, N. *Synth. React. Inorg., Met.-Org., Nano-Met. Chem.* **2008**, *38*, 18–24.
- (49) (a) Becke, A. D. *Phys. Rev. A* **1988**, *38*, 3098–3100. (b) Becke, A. D. *J. Chem. Phys.* **1993**, *98*, 1372–1377. (c) Becke, A. D. *J. Chem. Phys.* **1993**, *98*, 5648–5652.
- (50) Zhao, Y.; Schultz, N. E.; Truhlar, D. G. *J. Chem. Theory Comput.* **2006**, *2*, 364–382.
- (51) Boys, S. F.; Bernardi, F. *Mol. Phys.* **1970**, *19*, 553–566.

- (52) Møller, C.; Plesset, M. S. *Phys. Rev.* **1934**, *46*, 618–622.
- (53) Zhao, Y.; Truhlar, D. G. *Theor. Chem. Acc.* **2008**, *120*, 215–241.
- (54) Chai, J.; Head-Gorden, M. *Phys. Chem. Chem. Phys.* **2008**, *10*, 6615–6620.
- (55) Frisch, M. J.; Trucks, G. W.; Schlegel, H. B.; Scuseria, G. E.; Robb, M. A.; Cheese man, J. R.; Montgomery, J. A.; Vreven, T., Jr.; Kudin, K. N.; Burant, J. C.; et al. *Gaussian 09*, Revision A.01; Gaussian, Inc.: Wallingford, CT, 2004.
- (56) Parthasarathi, R.; Elango, M.; Subramanian, V.; Sathyamurthy, N. *J. Phys. Chem. A* **2009**, *113*, 3744–3749.
- (57) Byl, O.; Liu, J.; Wang, Y.; Yim, W.; Johnson, J. K.; Yates, J. T. *J. Am. Chem. Soc.* **2006**, *128*, 12090–12097.
- (58) Biegler-Konig, F.; Schonbohm, J.; Derdau, R.; Bayles, D.; Bader, R. F. W. *AIM2000*, version 1; Bielefeld: Germany, 2000.
- (59) Chattaraj, P. K.; Bandaru, S.; Monda, S. *J. Phys. Chem. A* **2011**, *115*, 187–193.
- (60) Srivastava, H. K.; Sastry, G. N. *J. Phys. Chem. A* **2011**, *115*, 7633–7637.